Transfer characteristics of a thermosensory synapse in *Caenorhabditis elegans*

Anusha Narayan[a,b], Gilles Laurent[b,c], and Paul W. Sternberg[a,b,1]

[a]Howard Hughes Medical Institute and [b]Division of Biology, California Institute of Technology, Pasadena, CA 91125; and [c]Max Planck Institute for Brain Research, 60528 Frankfurt/Main, Germany

Contributed by Paul W. Sternberg, April 27, 2011 (sent for review February 13, 2011)

Caenorhabditis elegans **is a compact, attractive system for neural circuit analysis. An understanding of the functional dynamics of neural computation requires physiological analyses. We undertook the characterization of transfer at a central synapse in *C. elegans* by combining optical stimulation of targeted neurons with electrophysiological recordings. We show that the synapse between AFD and AIY, the first stage in the thermotactic circuit, exhibits excitatory, tonic, and graded release. We measured the linear range of the input-output curve and estimate the static synaptic gain as 0.056 (<0.1). Release showed no obvious facilitation or depression. Transmission at this synapse is peptidergic. The AFD/AIY synapse thus seems to have evolved for reliable transmission of a scaled-down temperature signal from AFD, enabling AIY to monitor and integrate temperature with other sensory input. Combining optogenetics with electrophysiology is a powerful way to analyze *C. elegans*' neural function.**

The compact nervous system, defined anatomy, and available system analysis tools such as genetic manipulations, ablations of individual neurons, and real-time monitoring of neural activity using Ca^{2+} imaging and electrophysiology combine to make *Caenorhabditis elegans* useful for neural circuit analysis. In particular, the static wiring diagram has been described from electron microscopy (EM) studies (1). These data, although invaluable, do not address issues of functional connectivity, such as integration, gain control, and the real-time processing of information. To begin addressing such questions, we characterize transfer at a *C. elegans* central synapse, by combining electrophysiological and optogenetic techniques. We focus on synapses between neurons known to contribute to thermotaxis. On a temperature gradient, worms accumulate at the temperature at which they were cultivated (T_{cult}) and track narrow isotherms near T_{cult} (2) for up to 8 h after starvation (3). A preliminary circuit, including neurons AFD, AIY, AIZ, and RIA, was mapped using laser ablation (4). Fig. 1*A* shows these neurons with some of their significant synaptic partners. AFD is the primary thermosensory neuron (4, 5) and is a precise sensor: Ca^{2+} imaging experiments show that above T_{cult}, AFD Ca^{2+} levels can reliably track sinusoidal temperature variations of 0.05 °C (6). AFD appears to code for changes in temperature above a set point; this response is bidirectional and adaptive (7). Electrophysiological experiments show that increases in temperature over the set point produce large depolarizations in AFD, whereas cooling hyperpolarizes the cell to a smaller extent (8). How is this information conveyed to the next stage of the circuit? EM data (1) used to determine synaptic connectivity (9) indicate that interneuron AIY is the primary postsynaptic partner of AFD. AIY also receives synaptic input from the other known thermosensory neuron, AWC (10), as well as sensory neurons AWA and AWB. Ca^{2+} imaging data from AIY show that it also turns "on" above a temperature set point, and responds in phase with the temperature stimulus variations (6). A high-temporal resolution picture of the synaptic activity at the AFD/AIY synapse would allow us to address questions of spatiotemporal integration, gain control, and transfer characteristics. We attempt to characterize transfer at the AFD/AIY synapse using established whole-cell electrophysiological recordings (11). Paired recordings are currently infeasible, given the small size of the neurons (2–4 μm) and the short average duration of recordings (order of minutes). Instead, we used remote optical stimulation using channelrhodopsin-2 (chR2), a light-activated cation channel (12–14). We limited expression of chR2, to the presynaptic neuron AFD, and visually identified postsynaptic neuron AIY for recording by the selective expression of GFP (Fig. 1*B*). We focus on this functional thermosensory subcircuit to address general issues of central synaptic transmission in C. *elegans*.

Results

Light-Evoked Response in AFD. There are two AFD neurons, AFDL and AFDR, and each synapses on both AIY neurons, AIYR and AIYL (8–12 points of synaptic contact) (9). We expressed chR2 under the *gcy-8* promoter exclusively in AFDL and AFDR, to depolarize AFD selectively and remotely. The chR2 channels appear distributed over both cell body and neurites (Fig. 1*B*, expression pattern of fluorescence tag on chR2). Worms were fed *all-trans* retinal (ATR), necessary for functional chR2. Using blue light, we evoked inward currents of up to 10 picoamperes (pA) and depolarizations of up to 40 mV (Fig. 1 *C* and *D*, *Top* traces) in AFD. Worms fed no ATR ($n = 5$ cells) or stimulated with red light ($n = 7$ cells) showed no evoked potentials or currents (Fig. 1 *C* and *D*, *Middle* and *Bottom* traces). We controlled AFD membrane current and potential reversibly for the duration of the light pulse (Fig. 1 *E* and *F*), and the decay of evoked responses were fit with a single exponential (Table S1). For a light pulse of constant intensity 348.5 μW/mm^2, the amplitude of the evoked depolarization varied from 20 to 40 mV, with an average value of 28.2 mV. A twofold range was also observed in the evoked current (Table 1). Three observations can probably account for this twofold variation. First, chR2 expression varied almost twofold across animals (fluorescence intensity of the YFP tag, pixel intensity mean = 39.83, SD = 10.03, $n = 45$ neurons). Although the strain was constructed using a chromosomally integrated transgene, we know neither the level of expression of the transgene in each animal, nor that of ATR uptake by each individual. We measured the correlation between light-evoked currents and depolarizations recorded from the same cell (a subset of experiments, $n = 14$). We found no strong correlation (correlation coefficient = 0.142) between the amplitude of optically induced currents and potentials, implying that ATR/chR2 expression levels are not the sole determinant of the variability in response. Second, AFD input resistance varies almost twofold (Table 1), and third, some variability in pipette resistance and recording quality was unavoidable. We varied the intensity of our light stimulation over five orders of magnitude and measured the corresponding AFD depolarization. Fig. 2*A* shows an example recording from AFD, in response to 500-ms light pulses of varying light intensity. The intensity values are normalized (1 = peak light intensity of 348.5 μW/mm^2). Membrane potential varied log-linearly with light intensity (Fig. 2*B*; $n = 7$ cells, $R^2 = 0.9434$). The value of holding potential will affect our transfer function, because the membrane may have different voltage-dependent regimes. The resting membrane voltage (V_m) of AFD has been reported to be

Author contributions: A.N., G.L., and P.W.S. designed research; A.N. performed research; A.N. analyzed data; and A.N., G.L., and P.W.S. wrote the paper.

The authors declare no conflict of interest.

[1]To whom correspondence should be addressed. E-mail: pws@caltech.edu.

This article contains supporting information online at www.pnas.org/lookup/suppl/doi:10.1073/pnas.1106617108/-/DCSupplemental.

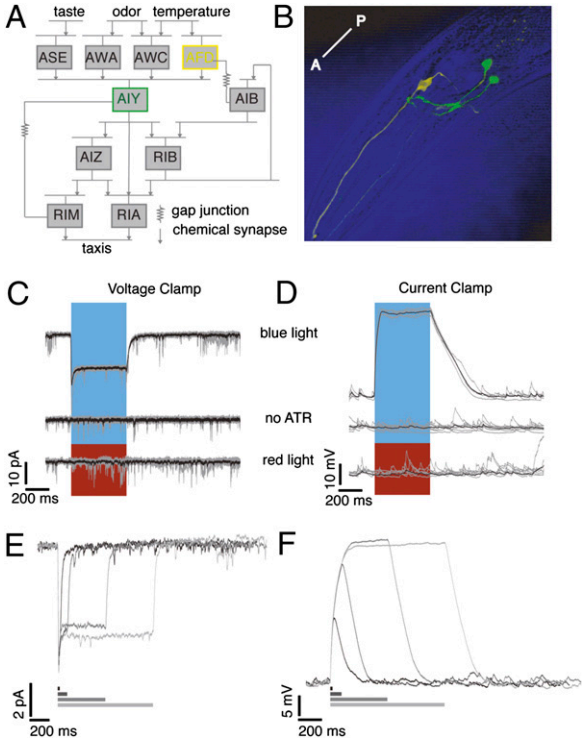

Fig. 1. Using chR2 to stimulate AFD, the primary thermosensory neuron in *C. elegans*. (*A*) Neurons involved in the thermosensory circuit and their synaptic partners. (*B*) Confocal image showing AFD neurons in yellow and AIY in green. The anterior-posterior (A-P) axis is as shown. (*C*) Voltage-clamp recordings from AFD, V_{hold} = −65 mV. A 500-ms pulse of blue light, and not red, causes inward current in AFD expressing functional chR2. *All-trans* retinal is required. Five trials from a single neuron in gray, average in black. (*D*) Current-clamp recordings from AFD in situations identical to *C*. V_m preceding the light pulse was ∼−65 mV. Light-evoked depolarization in AFD can be controlled reversibly. Example responses from a single neuron to 20-, 100-, 500-, and 1,000-ms light pulses in (*E*) voltage clamp and (*F*) current clamp.

∼−40 mV (8). A variety of resting potentials, ranging from −30 to −70 mV have been described for nonspiking neurons with graded synapses (15). Typically, these neurons tend to be more depolarized than spiking neurons. *C. elegans* neurons have high input resistance (a few gigaohms vs. hundreds of megaohms for larger neurons in other systems), resulting in a low seal resistance/input resistance ratio, which makes it difficult to obtain accurate measures of resting V_m. In the absence of true estimates of resting potential, we assessed the effect of holding potential by injecting current to subject AFD to different voltage values and measuring the evoked ChR2 depolarization. We maintained the AFD V_m at values from ∼+40 to ∼−100 mV and measured the response to a fixed light pulse at each step. The light-evoked depolarization in AFD varies as a function of holding potential (Fig. 2*C* shows an example neuron; Fig. 2*D* shows the variation of evoked potential with holding potential; seven trials from six neurons), and over the range of −30 to −70 mV, the evoked depolarization is 5–35 mV. This is comparable to the values we evoke with V_{hold} = ∼−65 mV.

Depolarization of AIY by Presynaptic, Light-Evoked Depolarization. We next stimulated AFD and recorded from AIY. Upon brief (20 ms, 348.5 mW/mm^2) light stimulation, we evoked postsynaptic currents (PSCs) and postsynaptic potentials (PSPs) of 0.5 pA and 3–5 mV, respectively (Fig. 3 *A* and *B*). Worms fed no ATR (n = 2) or stimulated with red light (n = 8) showed no evoked responses (Fig. 3 *A* and *B*, *Middle* and *Bottom* traces). The AIY response had slower kinetics than the chR2-evoked AFD response (Table S1). Because both AFD neurons each contact both AIY neurons, the recorded response in one AIY neuron probably resulted from aggregate synaptic input from two AFD neurons. The peak synaptic responses were small, and led us to explore the possibility that this was due not to the intrinsic size of the response, but instead to experimental conditions such as an imperfect voltage clamp (leading to unclamped outward conductances evoked by the PSP/depolarization). The results of substituting Cs^+ for K^+ in our pipette (n = 8 neurons) were inconclusive: in five of the recordings, the synaptic response was abolished; in the other three, it was not affected (Fig. S1). Another possible reason for the small size is that the neurite shunts away the synaptic current from the recording site (the soma). This is consistent with Ca^{2+} imaging results in which no significant changes in Ca^{2+} signal could be observed at the cell body of AIY, but only at a point along the neurite where it bends into the nerve ring (6, 16). Similar results have been reported for spiking neurons in the crab stomatogastric ganglion (17). For comparison, we analyzed spontaneous events occurring in AFD (see Fig. 1*C* baseline for examples; Fig. S2*C*). We investigated whether the origin of these events was synaptic by using genetic mutants. UNC-13 is a syntaxin-binding protein necessary for vesicle fusion (18, 19). The frequency of similar spontaneous events (Fig. S2 *A* and *B*, rightmost four graphs) in another amphid cell, ASER, is dramatically reduced in a *unc-13* (*s69*) background, but the frequency of such events in AFD itself was not reduced in a *unc-13* background (Fig. S2). In AFD, the spontaneous events were small [mean amplitude 2.3 mV, median 2 mV, interquartile range (IQR) 1.5 mV] and fast (mean rise time 5.6 ms, median 5.1 ms, IQR 4.4 ms, mean decay time 18.3 ms, median 17 ms, IQR 18.8 ms; Fig. S2*A*). The events in AFD could be synaptic in origin, but not *unc-13* mediated (perhaps mediated by the *unc-31* pathway). Another possibility is that these events originate from the voltage fluctuations of individual channels. We measure aggregate AFD/AIY synaptic activity, so the recorded excitatory postsynaptic potentials (EPSPs) must be multivesicular, which usually implies larger EPSPs and a wide range of composite decay times if release is asynchronous. Consistent with this, we see a wide distribution of decay times, albeit a fairly narrow range of sizes (Fig. S2*D*).

Release at the AFD/AIY Synapse Is Tonic. We stimulated AFD with light pulses of varying duration (Fig. 1 *E* and *F*). Fig. 3 *C* and *D*

Table 1. Average evoked responses and R_{in} values for AFD and AIY

	Peak evoked voltage						Peak evoked current						Mean input resistance					
			Mean	SD	Median	IQR			Mean	SD	Median	IQR			Mean	SD	Median	IQR
	n_{cells}	n_{trials}	(mV)				n_{cells}	n_{trials}	(pA)				n_{cells}	n_{trials}	(GOhm)			
AFD	24	129	31.6	6.2	31.9	8.1	19	104	15.34	11.79	12.48	6.51	28	162	3.99	3.99	2.59	2.3
AFD (T_{cult} = 15 °C)	6	49	10.4	3.2	10	4.1	4	65	7.61	1.14	7.73	1.09	8	114	5.07	5.03	3.38	4.54
AFD (T_{cult} = 25 °C)	9	116	26.3	9.6	26.4	13.4	10	145	27.73	10.11	29.05	19.1	10	261	7.09	2.98	2.02	2.45
AIY (wt) (T_{cult} = 20 °C)	20	100	2.3	0.8	2.3	1.3	21	99	0.44	0.17	0.43	0.26	21	199	4.32	1.8	3.93	2.79
AIY (*unc-31*)	6	68	2	0.91	2	0.88	4	34	0.15	0.06	0.17	0.99	6	102	7.05	1.33	6.65	1.75
AIY (*unc-13*)	4	34	2	1.2	2	1.1	4	20	0.32	0.11	0.29	0.15	4	54	5.89	0.63	6.03	1.08
AIY (T_{cult} = 15 °C)	8	98	1.3	1	1.2	1.8	8	119	0.2	0.16	0.16	0.11	7	217	8.9	5.7	7.74	2.1
AIY (T_{cult} = 25 °C)	11	83	2.5	1.6	2.1	2.6	11	142	0.33	0.17	0.3	0.12	11	225	7.8	1.8	7.6	2.4

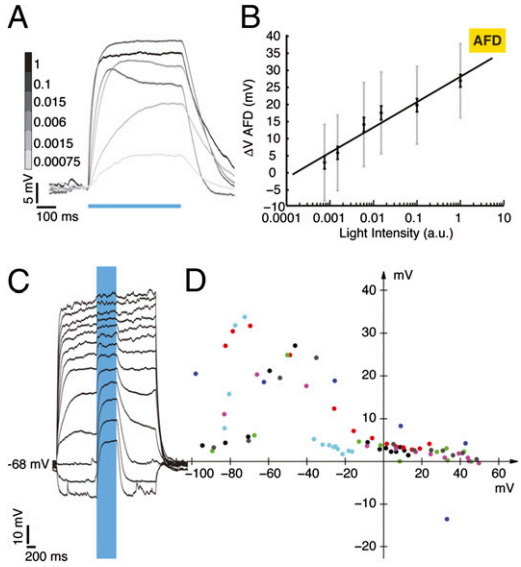

Fig. 2. Calibration of AFD response to blue light. (*A*) Depolarization evoked in AFD in response to five orders of magnitude variation in light intensity, 10-trial averages from example neuron. Light intensity is normalized, with one corresponding to a peak light intensity of 348.5 μW/mm^2. (*B*) Average evoked depolarization in AFD as a function of light intensity (gray bars SD, black bars SEM, n = 7 neurons). Response is log linear (R^2 = 0.9434). (*C*) Depolarization evoked in AFD as a function of holding potential, example recording. (*D*) Evoked potential as a function of holding potential. Seven trials from six neurons, coded by color for neuron. Two trials from one neuron are shown in black (acquired earlier in the recording) and gray (acquired later). Mean steady-state response in *B* and *D* measured by averaging the response over the second half of the light pulse.

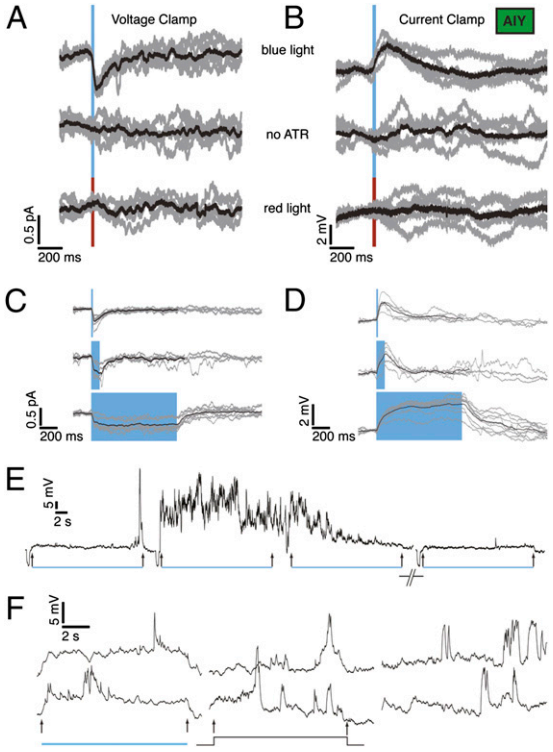

Fig. 3. Synaptic response in AIY is tonic. A 20-ms pulse of blue light is sufficient to evoke a synaptic response in AIY in voltage clamp (*A*) and current clamp (*B*). Controls show no response. Five trials from a single neuron in gray, average in black. Response of AIY is tonic (20-, 100-, and 1,000-ms light pulses). Voltage clamp (*C*) and current clamp (*D*). Five-trial averages of individual neurons in gray, average of all cells in black. The black average traces terminate early because some of the trials used to compute the average were shorter than others (*E*). AIY responses to long pulses of light. Four trials of AIY response to 20 s of blue light. A small hyperpolarizing pulse to measure R_{in} precedes each trial. (*F*) Example traces of AIY response to 10 s of blue light (*Left*, two trials), 10 s of 100-fA current injection (*Center*), and 10 s of no stimulus (*Right*). In all cases, V_m preceding the light pulse was ~−65 mV.

show evoked currents and potentials in AIY for three different pulse durations: 20 ms, 100 ms, and 1 s (with average responses from individual neurons in gray, and an all-cell average in black). Longer pulses (10 s; Fig. 3*F*, rightmost two traces) and up to 20 s (Fig. 3*E*) indicated a sustained component to the response. AFD response to long pulses (>1 s) was also sustained. The membrane of AIY displayed rich dynamics: we observed both depolarizing and repolarizing transients ranging in size from 5 to 25 mV. These transients were observable in the presence of blue light, with a 100-fA (femtoAmperes) current injection, and while holding the neuron close to presumed rest (Fig. 3*F*). The chR2-evoked component, though difficult to discern in individual trials, is clearly visible in a trial average (Fig. S3). To test if light evoked larger depolarizations in the presence of these transients, we computed the correlation between the amplitude of light-evoked depolarizations and frequency of spike-like transients. We found no significant correlation (correlation coefficient = 0.55, n = 4 neurons; Fig. S4). Additionally, the evoked depolarization in these cases (mean 1.9 mV, median 1.8 mV, IQR 0.7 mV, n = 4 neurons) is within the range of values from experiments where spike transients were absent.

Release at the AFD/AIY Synapse Is Graded. We varied light intensity over five orders of magnitude and measured the AIY synaptic response. Fig. 4*A* shows an example recording in response to 500-ms light pulses of varying light intensity. The intensity values are normalized (1 = peak light intensity of 348.5 μW/mm^2). Membrane potential varied log-linearly with light intensity (Fig. 4*B*, *Upper*; n = 4 neurons; R^2 = 0.6445). From the recordings shown in Figs. 2 and 4, we could extract an estimate of the soma-to-soma synaptic transfer function between AFD and AIY (Fig. 4*B*, *Lower*), with linear regression fit (regression coefficient = 0.056, R^2 = 0.69). This suggests an apparent gain of <0.1 mV of postsynaptic response for each millivolt of presynaptic depolarization within the range explored.

Synaptic Potential Reverses Between −20 and 0 mV. We stimulated the synapse while holding AIY at potentials between −100 and +40 mV (Fig. 4*C*; seven trials from four neurons). The synaptic potential appears to reverse between −20 and 0 mV (Fig. 4*D*). We attempted this experiment in voltage clamp; however, due to the small size of evoked currents, it was difficult to resolve changes with V_{hold}.

No Evidence of Facilitation or Depression at the AFD/AIY Synapse. We stimulated the synapse with trains of pulses ranging in width and intervals from 20 ms to 1 s. We observed no significant change in the size of the synaptic response (example traces in Fig. 5 *A*–*C*). We computed the evoked response to each pulse as the average over the second half of the pulse. We calculated the ratio of the first evoked potential to the average of the subsequent potentials (each measured as the mean of the second half of the light response) and compared these across different interpulse intervals; we found no clear trend. We also computed the ratio of the slope of the rising phase of the first pulse to the average of the succeeding ones; here, we found a decreasing trend that was mirrored in both pre- and postsynaptic neurons (Fig. 5 *B* and *C*, *Right*). We conclude that there is no frequency dependence in the evoked potential and no obvious facilitation or depression, at least within this range.

Transmission at the AFD/AIY Synapse Is *unc-31* Dependent. We attempted to identify the neurotransmitter used at the AFD/AIY synapse by recording from *unc-13* and *unc-31* mutants. *unc-13*

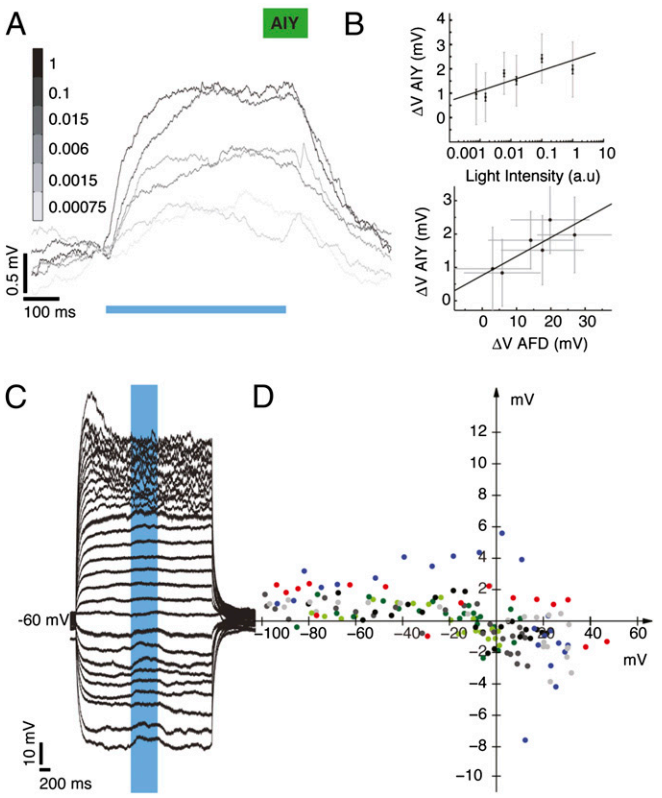

Fig. 4. AIY synaptic response is graded and reverses between −20 and 0 mV. (*A*) Depolarization evoked in AIY in response to five orders of magnitude variation in light intensity, 10-trial averages from example neuron. (*A Top*) Average evoked depolarization in AIY as a function of normalized light intensity (1 = peak light intensity of 348.5 μW/mm^2). Gray bars indicate SD, black bars SEM. Response is log linear (R^2 = 0.6445, n = 4 neurons). (*Bottom*) Transfer function of the AFD/AIY synapse. Average evoked depolarization in AIY as a function of average evoked depolarization in AFD. Gray bars indicate SD, R^2 = 0.69. (*C*) Reversing the AIY synaptic potential. Example recording, AIY held at different potentials. (*D*) Evoked synaptic depolarization as a function of holding potential, seven trials from four neurons, coded by color for neuron. Three trials from one neuron are labeled in black and dark and light gray (in chronological order). Two trials from another neuron are labeled in dark and light green. The black dots in *D* correspond to the data in *C*.

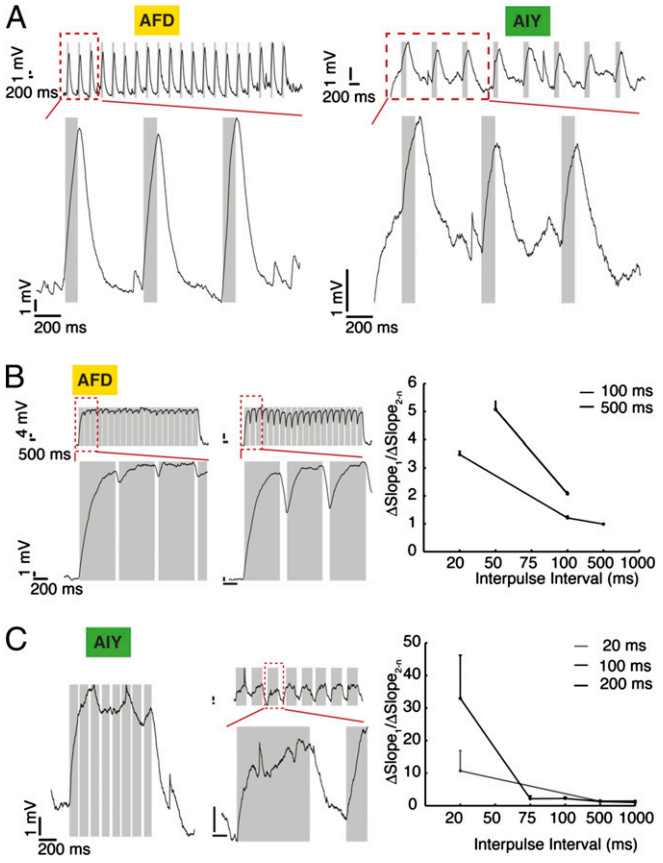

Fig. 5. AFD and AIY response to different pulse stimulation protocols: no evidence for facilitation and depression. (*A*) Example traces of AFD (*Left*) and AIY (*Right*) responses to light pulse trains (2 s). (*Upper*) Entire sequence of pulses. (*Lower*) Zoom of red boxed section of *Upper* trace. Pulse width, interval values: 100 ms, 500 ms. (*B*) AFD response. (*Left and Center*) More examples. Pulse width, interval values: *Left*, 500 ms, 50 ms; *Center*, 500 ms, 100 ms. (*Right*) Variation in ratio of slope of first evoked pulse to averaged slope of subsequent pulses in AFD. There is a decrease in the ratio of slopes with increasing pulse intervals (data pooled from three neurons). (*C*) AIY response, more examples: *Left*, 100 ms, 20 ms; *Center*, 1,000 ms, 500 ms. (*Right*) Variation in ratio of slope of first evoked pulse to averaged slope of subsequent pulses in AIY (data pooled from seven neurons). The decrease in the slope ratio across pulse train intervals in AFD is mirrored in AIY. Values are mean ± SEM.

encodes a syntaxin-binding protein necessary for fast synaptic transmission (18, 19), and *unc-31* encodes Ca^{2+}-dependent activator protein for secretion (CAPS), a protein required for dense-core vesicle exocytosis but not clear-vesicle synaptic transmission (20). There was a significant decrease in evoked currents in *unc-31* animals (reduced to 30% of wild type), whereas the currents in *unc-13* animals were not significantly altered (Fig. 6 *A* and *C*; Table 1). The *unc-31* mutation reduces but does not eliminate peptide release, so a partial deficit is the expected result at a peptidergic synapse (21). There was no significant difference in evoked potentials between *unc-13*, *unc-31*, and wild-type animals (Fig. 6 *B* and *D*; Table 1). Ohm's law can partially explain how a smaller-than-wild-type current could lead to a similar-to-wild-type potential in *unc-31* animals, because the measured R_{in} for the synaptic mutants is significantly higher than wild type [>1.5×, Table 1; ANOVA: $F(2, 91) = 24.25$; $P = 3.6164e\text{-}09$]; however, this does not explain why the *unc-13*–evoked potentials are not larger than wild type. These data suggest that the synaptic response in AIY is mediated by the *unc-31*–dependent dense-core vesicle pathway, and not the *unc-13*–mediated clear-vesicle pathway. Release at the AFD/AIY synapse is thus probably peptidergic.

Effect of Cultivation Temperature on AFD/AIY Transmission. We raised worms at different values of T_{cult} (15 °C, 20 °C, 25 °C) and recorded from AIY at 20 °C (Fig. S5 *A* and *B*, example traces, and Fig. S5*C*, population data). Synaptic currents in AIY were significantly reduced when T differed from T_{cult}. Synaptic potentials in AIY were significantly smaller when $T < T_{cult}$. To determine if these data can be explained by variable activation of AFD, we recorded from AFD in worms grown at different T_{cult}. We found that the evoked current and potential increased with increasing values of T_{cult} (Fig. S5*D*, *Upper*, example traces; *Lower Left* and *Lower Center*, population data). We tested the possibility that the ChR2 conductance varied with T_{cult} by quantifying the intensity of YFP expression in AFD at different T_{cult} (Fig. S5*D*, *Lower Right*). The mean fluorescence intensity at T_{cult} = 25 °C was significantly higher than both that at T_{cult} = 20 °C and T_{cult} = 15 °C, which confounded our analysis of the effect of varying T_{cult}, and underscores the necessity for calibration.

Discussion

Our experiments replaced the effects of temperature on AFD, our presynaptic neuron, with light/ChR2-evoked depolarization. How relevant were our presynaptic stimulation levels to those that AFD experiences under the effect of temperature changes in

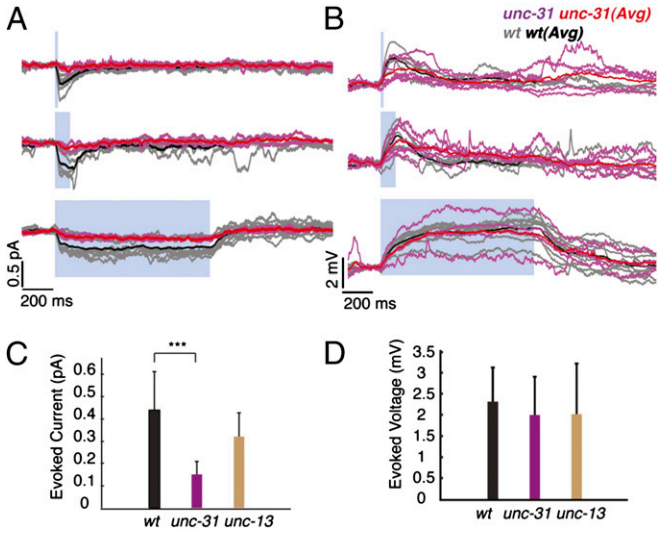

Fig. 6. The *unc-31* pathway mediates neurotransmission at the AFD/AIY synapse. (*A*) Evoked synaptic current is greatly reduced in a *unc-31* synaptic mutant but not in a *unc-13* mutant. (*B*) Evoked potential is unaltered in both *unc-31* and *unc-13* mutants. Five-trial average from example neuron recorded in a *unc-31* (pink), *unc-13* (brown), and wild-type (black) background. (*C*) Synaptic current is significantly reduced in a *unc-31* but not in a *unc-13* background [ANOVA: $F(2, 40) = 15.8423$, $P = 8.5640\text{e-}06$] post hoc Tukey's honestly significant difference (HSD) tests]. $n_{unc\text{-}13} = 4$, $n_{unc\text{-}31} = 4$, $n_{wt} = 21$ neurons. (*D*) Synaptic potential is not significantly different between mutants and wild type [ANOVA: $F(2, 48) = 0.6734$, $P = 0.5147$]. $n_{unc\text{-}13} = 4$, $n_{unc\text{-}31} = 6$, $n_{wt} = 20$ neurons. All values are mean ± SD; values in *C* and *D* are evoked response averaged over all pulse durations, measured as follows: 20-ms pulses, the peak evoked response; 100-ms and 1-s pulses: average response over the second half of the light pulse.

vivo? Previous work (8) showed that AFD responds to changes in temperature with inward currents between 1 and 19 pA and depolarization of 40 mV when $T > T_{cult}$, with an average latency of activation of 96 ± 5 ms. These values are comparable to our ChR2-mediated responses in AFD. With stimulation in this range, we find that the AFD/AIY synapse is graded and tonic, with a faithful rendering of ΔT from AFD to AIY.

The first graded central synapses to be characterized electrophysiologically were in arthropods (22–26). Graded synapses are characterized by sustained release and a low voltage threshold. Spiking neurons can also have graded synapses (e.g., the L-neuron in the locust ocellar visual system (27) and spiking motor neurons in the lobster stomatogastric ganglion) (28). Sustained release can last for several minutes (>5 min between locust ocellar L-neurons and third-order neurons) (29) or, in cases where the resting V_m is depolarized above neurotransmitter release threshold, possibly indefinitely—for example, the locust L-neurons (29) and nonspiking neurons in locust thoracic ganglia (24). Sustained release in vertebrate-graded synapses (e.g., in the retina and cochlea) is correlated with the presence of ribbons (30) and fast replenishment of a large vesicle pool (31). However, central nonspiking synapses in the locust do not possess ribbons (32). Release at the AFD/AIY synapse could be sustained for as long as 20 s (Fig. 3 *E* and *F*). EM data (1) show no evidence of the existence of ribbon synapses in *C. elegans*, but indicate that there are multiple release sites between AFD and AIY (9), which might explain the sustained response. Graded synapses such as the EX1-GM synapse in the lobster's stomatogastric ganglion (25) show multicomponent postsynaptic responses, which might involve presynaptic conductance changes and/or postsynaptic desensitization. We observed declining postsynaptic responses with long (≥10 s) light-induced presynaptic depolarization, consistent with desensitization. A low release threshold implies that bidirectional membrane fluctuations can cause modulations of transmitter release and thus, postsynaptic responses (23). Previous work suggests that AFD V_m can be reset by temperature changes in either direction (8). Whether this modulates neurotransmitter release in vivo depends on the overlap between the normal range of the presynaptic voltage and that of release at the synapse, and we do not yet know the true resting potential and V_m range for AFD in vivo. Though our population data suggests a likely reversal potential between −20 and 0 mV, we were unable to clearly reverse the synaptic potential in AIY, even though we subjected the neuron to a wide range of holding potentials. One possible reason could be electrical shunting by the neurite: other studies have reported stimulus-evoked changes in Ca^{2+} at a spot further along the neurite in the absence of significant Ca^{2+} transients at the AIY soma (6, 16). The small evoked current and filtered shape of our recorded potential lend credence to the shunting hypothesis. There are other possible reasons for incomplete reversal: first, activation of large outward conductances by holding the cell at large positive values of membrane potentials. Experiments in voltage clamp show a variety of inward and outward currents that activate at depolarized values (Fig. S6). Second, the response at AIY could be due to a highly rectifying channel (e.g., the strongly rectifying graded synapse between rods and horizontal cells in tiger salamander retina clips the signal above a certain amplitude) (33). Third, we could be inadequately clamping the synapse due to improper space clamp. Thermotaxis has a glutamate-mediated component: worms carrying a mutation in the vesicular glutamate transporter *eat-4* show a weakened cryophilic response above T_{cult} (7), and there is evidence that AFD action inhibits AIY through glutamate, possibly countering the actions of another (unknown) neurotransmitter whose action from AFD to AIY is excitatory (34). We suggest that this neurotransmitter is a peptide, because the postsynaptic response requires the presence of UNC-31 (CAPS), but not UNC-13. This is consistent with the fact that AFD is known to produce several neuropeptides (35). The sign of the effect of AFD onto AIY has been the subject of speculation (4). Our experiments establish that the net transfer between AFD and AIY is excitatory, with an apparent compound reversal potential between −20 and 0 mV, consistent with a mixed cationic conductance. Existing EM data (1, 9) provide evidence for chemical synapses but not for gap junctions between AFD and AIY; we show that the postsynaptic response has a reversal potential and is dependent on the *unc-31* signaling pathway, indicating that the synapse is, at least in part, chemical in nature and probably peptidergic. Our efforts to determine how the AFD/AIY signaling varied when $T \neq T_{cult}$ were confounded by the temperature dependence of ChR2 expression. The AIY response remained unchanged or decreased slightly between $T_{cult} = 20\,°C$ and $T_{cult} = 25\,°C$, despite the fact that the AFD currents increased. The fact that the response of AIY did not increase could represent some upper bound in the release capacity of this synapse, or a ΔT-dependent modification of the synaptic gain (where $\Delta T = T - T_{cult}$). We could characterize transfer at the AFD/AIY synapse only in its linear range; technical and biophysical constraints prevented us from measuring threshold and saturation. As in other synapses (e.g., lobster stomatogastric ganglion) (25), this range of the input-output curve allowed us to estimate its peak (apparent) gain: gain at the AFD/AIY synapse was low (around 0.1). Gain factors of <1 are not uncommon; at locust nonspiking synapses, such as that between the ocellar L-neuron and a third-order neuron, transfer gain is ∼1, consistent with the fact that the third-order neuron integrates information from multiple sources (36). High-gain synapses imply high sensitivity and high signal-to-noise ratio; they must, however, be paired with some form of adaptation so as to maintain a large operating range, e.g., blowfly photoreceptor synapses (gain = 6) (37), and the locust ocellar synapses (gain = 20) (36).

What do our results imply for the functional and computational role of this synapse? The fact that the AIY response is tonic, shows no adaptation, and is frequency independent over the range of inputs explored would suggest that the role of this synapse is to provide AIY with a faithful scaled-down version of temperature changes tracked by AFD. The low gain at this synapse is also consistent with the presumed integrative role played by AIY, which processes multiple streams of sensory information. In our results, AIY responses are graded, but the range is fairly com-

pressed. Thus, AIY may not make the most of the analog information encoded in the amplitude of the synaptic input from AFD. There is precedent for this: at the synapse between nonspiking neurons 151 and mechanosensory P-neurons in the leech (38), the maximum amplitude of the synaptic potential is similar over the range of behaviorally relevant input frequencies, and information appears to be coded primarily in the duration of the depolarization and the time to reach peak amplitude. Nonspiking local interneurons in the locust implement an adaptive gain control mechanism through the matching of synaptic and membrane nonlinearities (39). This gain control has the effect of linearizing polysynaptic pathways, and presenting information to downstream neurons in a context-independent way. Such mechanisms, if used at the AFD/AIY synapse, would allow it to isolate and process thermosensory information in a separate channel, ensuring a reliable and accurate representation of the thermal environment. The small synaptic responses in AIY coupled with the presence of large depolarizing transients (Fig. 3 *E* and *F*) raises interesting questions regarding the processing further downstream, such as what causes AIY to release neurotransmitters in turn, how it integrates information from AFD with inputs from other chemosensory neurons, and whether it needs conjunctive neuronal input or long-range neuromodulatory influences to be activated. ChR2 has been used as a tool to study synaptic transfer at the *C. elegans* neuromuscular junction (40, 41). We have successfully applied this method to the characterization of a central synapse in *C. elegans*. Together, these studies establish the use of ChR2 as an effective tool in the analysis of the neural circuitry of the worm. The use of optical stimulation techniques in combination with physiology can serve as a powerful tool in our efforts to understand how the remarkably compact *C. elegans* nervous system processes information to shape a worm's response to its environment.

Materials and Methods

Electrophysiology: internal buffer contained 143 mM KAsp, 0.1 mM $CaCl_2$, 1.1 mM EGTA, 10 mM Hepes, 15 μM sulforhodamine, 4 mM MgATP, 0.5 mM Na_3GTP with pH 7.2 and osmolarity ~310 mOsm. Cs^{2+} solutions were made by substituting those ions for K^+; external buffer consisted of 145 mM NaCl, 5 mM KCl, 5 mM $MgCl_2$, 1 mM $CaCl_2$, 10 mM Hepes with pH 7.2 and osmolarity ~320 mOsm.

ACKNOWLEDGMENTS. We thank Serge Faumont, Thad Lindsay, and Shawn Lockery for their generous aid with the *C. elegans* preparation and helpful discussions. We thank Vivek Jayaraman, Glenn Turner, and members of the G.L. and P.W.S. laboratories for helpful discussions, the Caenorhabditis Genetics Center for strains, and WormBase. This work was supported by the Howard Hughes Medical Institute, with which P.W.S. is an investigator.

1. White JG, Southgate E, Thomson JN, Brenner S (1986) The structure of the nervous system of the nematode *Caenorhabditis elegans*. *Philos Trans R Soc Lond B Biol Sci* 314:1–340.
2. Hedgecock EM, Russell RL (1975) Normal and mutant thermotaxis in the nematode *Caenorhabditis elegans*. *Proc Natl Acad Sci USA* 72:4061–4065.
3. Luo L, Clark DA, Biron D, Mahadevan L, Samuel AD (2006) Sensorimotor control during isothermal tracking in *Caenorhabditis elegans*. *J Exp Biol* 209:4652–4662.
4. Mori I, Ohshima Y (1995) Neural regulation of thermotaxis in *Caenorhabditis elegans*. *Nature* 376:344–348.
5. Kimura KD, Miyawaki A, Matsumoto K, Mori I (2004) The *C. elegans* thermosensory neuron AFD responds to warming. *Curr Biol* 14:1291–1295.
6. Clark DA, Biron D, Sengupta P, Samuel AD (2006) The AFD sensory neurons encode multiple functions underlying thermotactic behavior in *Caenorhabditis elegans*. *J Neurosci* 26:7444–7451.
7. Clark DA, Gabel CV, Lee TM, Samuel AD (2007) Short-term adaptation and temporal processing in the cryophilic response of *Caenorhabditis elegans*. *J Neurophysiol* 97: 1903–1910.
8. Ramot D, MacInnis BL, Goodman MB (2008) Bidirectional temperature-sensing by a single thermosensory neuron in *C. elegans*. *Nat Neurosci* 11:908–915.
9. Chen BL, Hall DH, Chklovskii DB (2006) Wiring optimization can relate neuronal structure and function. *Proc Natl Acad Sci USA* 103:4723–4728.
10. Kuhara A, et al. (2008) Temperature sensing by an olfactory neuron in a circuit controlling behavior of *C. elegans*. *Science* 320:803–807.
11. Goodman MB, Hall DH, Avery L, Lockery SR (1998) Active currents regulate sensitivity and dynamic range in *C. elegans* neurons. *Neuron* 20:763–772.
12. Nagel G, et al. (2005) Light activation of channelrhodopsin-2 in excitable cells of *Caenorhabditis elegans* triggers rapid behavioral responses. *Curr Biol* 15:2279–2284.
13. Boyden ES, Zhang F, Bamberg E, Nagel G, Deisseroth K (2005) Millisecond-timescale, genetically targeted optical control of neural activity. *Nat Neurosci* 8:1263–1268.
14. Nagel G, et al. (2003) Channelrhodopsin-2, a directly light-gated cation-selective membrane channel. *Proc Natl Acad Sci USA* 100:13940–13945.
15. Siegler MVS (1984) Local interneurones and local interactions in arthropods. *J Exp Biol* 112:253–281.
16. Chalasani SH, et al. (2007) Dissecting a circuit for olfactory behaviour in *Caenorhabditis elegans*. *Nature* 450:63–70.
17. Ross WN, Graubard K (1989) Spatially and temporally resolved calcium concentration changes in oscillating neurons of crab stomatogastric ganglion. *Proc Natl Acad Sci USA* 86:1679–1683.
18. Madison JM, Nurrish S, Kaplan JM (2005) UNC-13 interaction with syntaxin is required for synaptic transmission. *Curr Biol* 15:2236–2242.
19. Richmond JE, Davis WS, Jorgensen EM (1999) UNC-13 is required for synaptic vesicle fusion in *C. elegans*. *Nat Neurosci* 2:959–964.
20. Speese S, et al. (2007) UNC-31 (CAPS) is required for dense-core vesicle but not synaptic vesicle exocytosis in *Caenorhabditis elegans*. *J Neurosci* 27:6150–6162.
21. Zhou KM, et al. (2007) PKA activation bypasses the requirement for UNC-31 in the docking of dense core vesicles from *C. elegans* neurons. *Neuron* 56:657–669.
22. Maynard DM, Walton KD (1975) Effects of maintained depolarization of presynaptic neurons on inhibitory transmission in lobster neuropil. *J Comp Physiol A Neuroethol Sens Neural Behav Physiol* 97:215–243.
23. Burrows M, Siegler MV (1976) Transmission without spikes between locust interneurones and motoneurones. *Nature* 262:222–224.
24. Burrows M, Siegler MV (1978) Graded synaptic transmission between local interneurones and motor neurones in the metathoracic ganglion of the locust. *J Physiol* 285:231–255.
25. Graubard K (1978) Synaptic transmission without action potentials: input-output properties of a nonspiking presynaptic neuron. *J Neurophysiol* 41:1014–1025.
26. Juusola M, French AS, Uusitalo RO, Weckström M (1996) Information processing by graded-potential transmission through tonically active synapses. *Trends Neurosci* 19:292–297.
27. Simmons P (1982) Transmission mediated with and without spikes at connexions between large second-order neurones of locust ocelli. *J Comp Physiol A Neuroethol Sens Neural Behav Physiol* 147:401–414.
28. Graubard K, Raper JA, Hartline DK (1980) Graded synaptic transmission between spiking neurons. *Proc Natl Acad Sci USA* 77:3733–3735.
29. Simmons PJ (1981) Synaptic transmission between second- and third-order neurones of a locust ocellus. *J Comp Physiol A Sensory Neural Behav Physiol* 145:265–276.
30. Sterling P, Matthews G (2005) Structure and function of ribbon synapses. *Trends Neurosci* 28:20–29.
31. Griesinger CB, Richards CD, Ashmore JF (2005) Fast vesicle replenishment allows indefatigable signalling at the first auditory synapse. *Nature* 435:212–215.
32. Watson AH, Burrows M (1988) Distribution and morphology of synapses on nonspiking local interneurones in the thoracic nervous system of the locust. *J Comp Neurol* 272:605–616.
33. Attwell D, Borges S, Wu SM, Wilson M (1987) Signal clipping by the rod output synapse. *Nature* 328:522–524.
34. Ohnishi N, Kuhara A, Nakamura F, Okochi Y, Mori I (2011) Bidirectional regulation of thermotaxis by glutamate transmissions in *Caenorhabditis elegans*. *EMBO J* 30: 1376–1388.
35. Colosimo ME, et al. (2004) Identification of thermosensory and olfactory neuron-specific genes via expression profiling of single neuron types. *Curr Biol* 14:2245–2251.
36. Simmons PJ (1999) The performance of synapses that convey discrete graded potentials in an insect visual pathway. *J Neurosci* 19:10584–10594.
37. Laughlin SB, Howard J, Blakeslee B (1987) Synaptic limitations to contrast coding in the retina of the blowfly Calliphora. *Proc R Soc Lond B Biol Sci* 231:437–467.
38. Marín-Burgin A, Szczupak L (2000) Processing of sensory signals by a non-spiking neuron in the leech. *J Comp Physiol A Neuroethol Sens Neural Behav Physiol* 186:989–997.
39. Laurent G (1993) A dendritic gain control mechanism in axonless neurons of the locust, Schistocerca americana. *J Physiol* 470:45–54.
40. Liu Q, Hollopeter G, Jorgensen EM (2009) Graded synaptic transmission at the *Caenorhabditis elegans* neuromuscular junction. *Proc Natl Acad Sci USA* 106:10823–10828.
41. Liewald JF, et al. (2008) Optogenetic analysis of synaptic function. *Nat Methods* 5: 895–902.